ACS APPLIED POLYMER MATERIALS

pubs.acs.org/acsapm Article

Anisotropic Hydrogels with Multiscale Hierarchy Based on Ionic Conductivity for Flexible Sensors

Xie Fu,*,⊥ Hui Tong,⊥ Xia Zhang, Kun Zhang, Lyes Douadji, Shuai Kang, Jinling Luo, Ziwei Pan, and Wenqiang Lu*

Cite This: ACS Appl. Polym. Mater. 2023, 5, 9876−9887 Read Online

ACCESS | Metrics & More | Article Recommendations | Supporting Information

ABSTRACT: Nature materials (skin, tissue, plant fiber, and nacre) exhibit super strength and toughness attributed to their unique multiscale hierarchical anisotropic structure. Hydrogels with excellent flexibility, adjustability, and good biocompatibility have become the exciting frontiers in soft electronics, while anisotropic hydrogels that mimic natural materials still face challenges. Herein, we fabricated an anisotropic poly(vinyl alcohol) hydrogel (DS-PVA) with a multiscale hierarchical structure (micro, submicron, and nano) by directional freezing versus salting out, which differs from isotropic hydrogel mechanical performance and force stimuli electrical response behavior. The PVA hydrogel parallel to the freezing direction (DS-PVA$_{\parallel}$) showed excellent strength 2.35 MPa (about five times DS-PVA$_{\perp}$), toughness 1712 KJ/M^3 (9.4 times DS-PVA$_{\perp}$), stability, and antifatigue characteristics, while the DS-PVA$_{\perp}$ indicated a higher sensitivity (GF = 4.4, ε = 5%) and a faster response/recovery time (127 ms/63 ms). These hydrogels, similar to natural materials with anisotropic mechanical properties, asymmetric sensing properties, and directional recognition, will provide a strategy for flexible sensor applications.

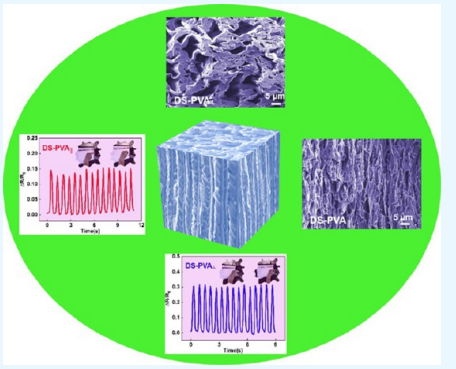

KEYWORDS: *anisotropic hydrogel, flexible sensor, directional freezing, multiscale hierarchical structure, ionic conductive*

1. INTRODUCTION

Soft electronics have emerged as an exciting frontier in research hotspots, including multiple disciplines of physics, chemistry, material, medicine, and biology.[1−3] It has been widely studied in flexible sensors, electronic skins, soft robots, and human−machine interfaces due to the soft electronic virtues of great twist ability, bendability, and foldability.[4−7] With high water contents, good conductivity, and mechanical performance, conductive hydrogels are promising candidates for soft electronics.[8,9] The conductive hydrogel is the intermediate state between solid and liquid, endowing an adjustable structure and more functional properties. However, most traditional conductive hydrogels have simple structures and poor mechanical properties. So there are many efforts between the structure designs and hydrogel properties, such as single-network hydrogels,[10,11] double-network hydrogels,[12,13] and cross-linking hydrogels.[14,15] Many attempts have been made in the conductivity of hydrogels, such as introducing conductive polymers,[16] ions,[17] ionic liquids,[18] and nano-conductive fillers (graphene, MXenes, and carbon nanotubes).[19−21]

Despite this, conductive hydrogels' structure, properties, and biocompatibility are certainly different from human tissues and muscles. Nature materials such as skins, tissues, skeletons, plant fibers, and nacre with super strength and toughness are attributed to the unique hierarchical structure with multiscale lengths (microfibers, submicron fibers, and nanofibers).[22] Recently, many methods have been developed to construct anisotropic conductive hydrogels that mimic natural materials, such as electronic and magnetic alignment,[23,24] mechanical stretching,[25,26] additional fillers,[27] and directional freezing.[28−30] All of these methods are based on the hydrogel molecular chain orientation along a certain direction to achieve an ordered structure and fabricate anisotropic hydrogels. These anisotropic hydrogels have a degree of discrepancy in mechanical performance between the parallel and vertical directions. Nevertheless, these anisotropic conductive hydrogels still cannot fully simulate natural materials due to the lack of a certain molecular chain or aggregation structure in series without the multiscale hierarchical structure. Therefore, many problems still must be solved in the fabrication of conductive anisotropic hydrogels with multiscale hierarchical structures.

Based on this, Zhai et al.[31] prepared a multiscale hierarchical structure of fibrous hydrogels by freeze-casting, solvent substitution, and ion enhancement. Then, the relationship

Received: July 20, 2023
Revised: October 12, 2023
Accepted: October 16, 2023
Published: November 8, 2023

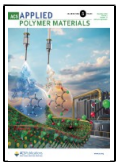

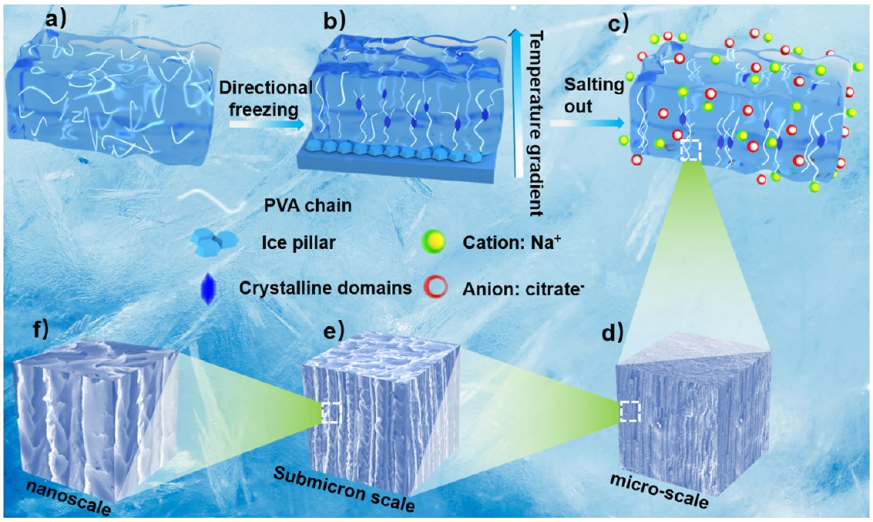

Figure 1. Fabrication of the multiscale hierarchical structure and anisotropic PVA hydrogel based on the directional freezing-assisted salting-out effect. (a) Disorderly distributed PVA solution; (b) PVA molecular chains arranged in order after directional freezing; (c) adjustment of PVA aggregation for the salting-out effect; (d) micrometer-scale structure diagram; (e) submicrometer-scale structure diagram; (f) nanoscale structure diagram.

between mechanical properties and morphological structure by the finite element method was systematically analyzed. He et al.[32] reported anisotropic hydrogels with micrometer-scale honeycomb-like pore walls containing nanofibril mesh interconnection based on freeze-casting and salting-out methods. These hydrogels exhibit excellent mechanical properties, and their structures are similar to those of natural materials. In addition, this hydrogel, mimicking the natural material-like structure, not only shows super flexibility and wearability similar to traditional flexible sensors but also solves the defects of the single signal output of traditional flexible sensors to a certain extent.[33] Traditional flexible sensors generally output a single strain response signal, which does not have directional selectivity. In fact, the sensing response system exhibits complex response behavior patterns such as response asymmetry and directionality.[34] For example, the detection of complex activities of body joints (such as the finger, wrist, neck, mouth, etc.) shows different tactile sensing, multiple statuses, and complexity. Therefore, these structure materials mimicking nature materials in soft electronic applications must be systematically studied to construct an evolutionary relationship among the internal structure, mechanical properties, and sensing performance of the hydrogels similar to natural materials.

Here, we prepared a PVA conductive hydrogel with an anisotropic multiscale hierarchical structure by directional freezing versus citrate solution salting-out effect (DS-PVA). The PVA molecular chain occurred at orientation with loading the temperature gradient field, resulting in a millimeter-scale, micron-level aggregate orientation structure. Then, under the anion salting-out effect (Hofmeister effect), the PVA aggregation states would be further altered, resulting in PVA molecular chains self-coalesced, forming the nanofibrils.[35] Moreover, such conductive hydrogel's mechanical properties and sensing performance were analyzed to establish the evolution between material morphologies and macroscopic properties.

2. EXPERIMENTAL SECTION

2.1. Materials. Poly(vinyl alcohol) (PVA-124) with a 54−66 mPa●s viscosity and MW 44.05 was purchased from Shanghai Aladdin Biochemical Technology Co., Ltd. Shanghai Aladdin Biochemical Technology Co., Ltd., provided sodium citrate ($C_6H_5Na_3O_7{\cdot}2H_2O$) with a 294.1 MW. Chongqing Rio Tinto Gas Co., Ltd., supplied liquid nitrogen.

2.2. Specimen Preparation. *2.2.1. Fabrication of the Multiscale Hierarchical Anisotropic Hydrogel (DS-PVA).* First, PVA-124 was dissolved into demi water to prepare the PVA solution (2, 5, and 10%). Then, the PVA solution was poured into a container made of PTFE (insulation layer) and copper bottom (heat transfer layer), which was placed on the top of the copper block, and the top exposed 1 cm of liquid nitrogen. The rest was immersed in liquid nitrogen and frozen in the direction for 30 min (Figure S1). Finally, the frozen samples were immersed in sodium citrate solution with 10, 15, 20, 25, 30, and 40% concentrations for 24 h to get the hydrogels.

2.2.2. Fabrication of the Cyclic Freeze−Thaw Hydrogel (CT-PVA). The PVA-124 was dissolved into demi water to prepare a 5% PVA solution. Then, the solution was cast into the module and froze for 30 min. After that, the module was removed for thawing for 2 h. This cycle was operated five times to prepare the CT-PVA.

2.3. Characterization. *2.3.1. Tensile Test.* The multiscale hierarchical anisotropic hydrogels were cut into dumbbell-shaped splines along the parallel and vertical freezing directions (DS-$PVA_{\parallel}$ and DS-$PVA_{\perp}$). The CT-PVA was also cut into dumbbell-shaped splines. Then, the specimens were measured with the universal tester (made in Instron, Series3360) operating in a tension mode at 23 ± 2 °C. A crosshead speed of 50 mm/min was used in the test.

2.3.2. Stress−Strain Electrical Response. The stress−strain electrical response analyzed the electrical response behavior of different strain hydrogels by combining a ball screw electric CNC platform with a Keithley 2450 digital source meter (Figure S2).

2.3.3. Fatigue Test. The universal tensile testing machine (ETM103B) was used to perform a 10% strain loading−unloading 10,000-cycle fatigue test on the hydrogel specimen.

2.3.4. SEM Analysis. The DS-$PVA_{\parallel}$ and DS-$PVA_{\perp}$ adopted liquid nitrogen brittle fractures were analyzed by scanning electron microscopy (SEM; S-4300, HITACHI). After loading 10, 100, 300, 500, and 800% strain, the DS-$PVA_{\parallel}$'s surface morphologies were analyzed by SEM. After loading 10, 30, 50, and 100% strain, the DS-$PVA_{\perp}$'s surface morphologies were analyzed by SEM. SEM analysis analyzed the fracture surfaces of DS-$PVA_{\parallel}$, DS-$PVA_{\perp}$, and CT-PVA.

https://doi.org/10.1021/acsapm.3c01626
ACS Appl. Polym. Mater. 2023, 5, 9876−9887

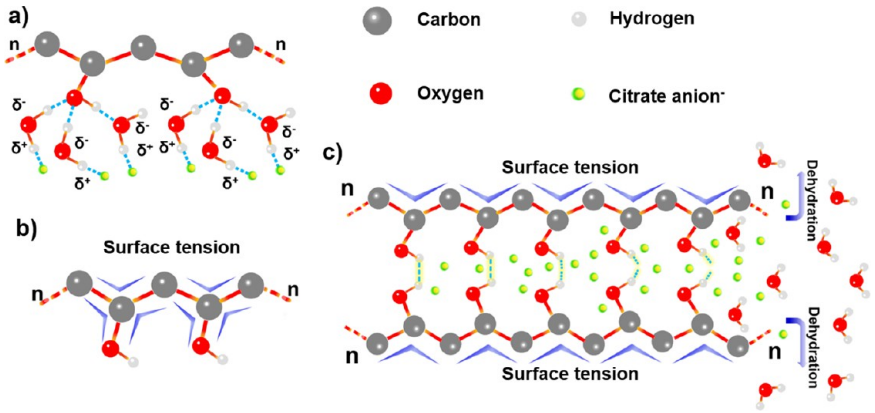

Figure 2. Regulation principle of the PVA molecular chain structure induced by the citrate anion due to the salting-out effect. (a) Interaction between the PVA chain and the water molecule; (b) interaction between the citrate anion and the PVA chain; (c) principle of aggregation among the PVA chain, citrate anion, and water molecule.

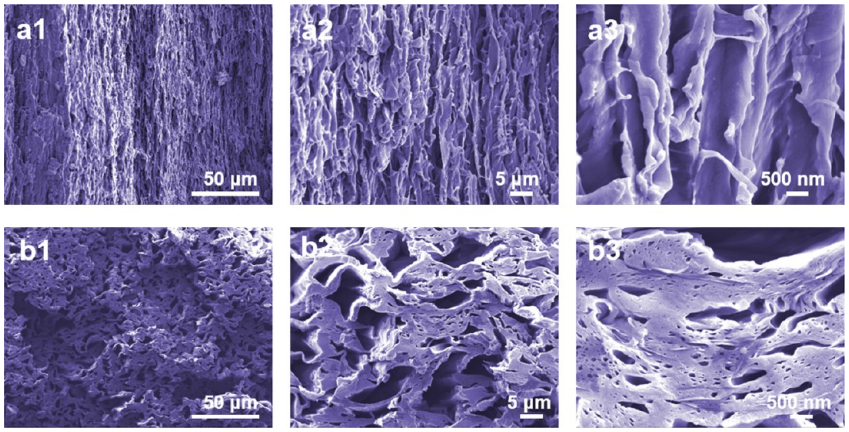

Figure 3. Morphology of DS-PVA in parallel and vertical freezing directions at different scales. (a1) Morphology of DS-PVA$_{\parallel}$ with a microscale; (a2) morphology of DS-PVA$_{\parallel}$ with a submicron scale; (a3) morphology of DS-PVA$_{\parallel}$ with a nanoscale; (b1) morphology of DS-PVA$_{\perp}$ with a microscale; (b2) morphology of DS-PVA$_{\perp}$ with a submicron scale; (b3) morphology of DS-PVA$_{\perp}$ with a nanoscale.

2.3.5. Transmittance Analysis. The transmittance of DS-PVA and CT-PVA in the visible light range (500−800 nm) was analyzed by a UV−visible spectrophotometer (Lambda 35).

2.3.6. Differential Scanning Calorimetry (DSC) Analysis. Before the DSC test, the CT-PVA and DS-PVA hydrogels were first freeze-dried under −70 °C and 300 Pa for 24 h in vacuum-drying equipment. Then, the glass transition temperature (T_g), crystallization temperature (T_C), and melting temperature (T_m) were analyzed by a differential scanning calorimeter (METTLER). Test conditions: temperature range, 0−250 °C; heating rate, 5 °C/min; gas atmosphere, N_2.

3. RESULTS AND DISCUSSION

3.1. Regulation Mechanism of the DS-PVA Aggregation Structure. Generally, the polymer solution was arranged disorderedly, and the gel was macroscopically isotropic (Figure 1a). While the PVA chains suffered the freeze with a temperature gradient, the molecular chains' order aligned, forming a crystal structure (Figure 1b). Then, the frozen PVA chains were soaked in sodium citrate, triggering penetration diffusion (Figure 1c). So, the citrate anion polarized the water molecule, inducing the destruction of the hydrogen bond between the water molecule and the hydroxyl group of the PVA molecular chain (Figure 2a). Meanwhile, the ions could increase the surface tension among the PVA molecular chains (Figure 2b). The salt effect could also break the hydrogen bonds among the PVA chains. Under surface tension, the PVA molecular chains would be more aggregated, and the water molecules between the molecular chains would be excluded, resulting in self-coalesce and phase separation (Figure 2c).[36,37] This way, the PVA phase morphology was reconstructed, forming a multiscale hierarchical anisotropic hydrogel, which showed the micro- and submicrometer-scale aligned pore wall (Figure 1d,e) and nanofibril (Figure 1f).

Figure 3 shows the SEM photos of DS-PVA with parallel and vertical directions for different scales. The morphologies exhibited a multiscale hierarchical structure similar to natural materials in parallel and vertical freezing directions. The PVA aggregation states aligned with the parallel temperature gradient direction (Figure 3a1). A similar pore wall structure appeared on a smaller scale (Figure 3a2). Furthermore, a nanofibril pore wall structure appeared on a 500 nm scale (Figure 3a3). In the vertical temperature gradient direction, the PVA morphologies showed porous structures with sizes ranging from micro- to nanoscales (Figure 3b1−b3). Such multiscale hierarchical anisotropic hydrogels are believed to differ greatly in direction for mechanical performance and sensing properties.

3.2. Relationship between Mechanical Properties and Morphological Structure. Directional freezing aligned PVA chains along the temperature gradient, resulting in microscale

https://doi.org/10.1021/acsapm.3c01626
ACS Appl. Polym. Mater. 2023, 5, 9876−9887

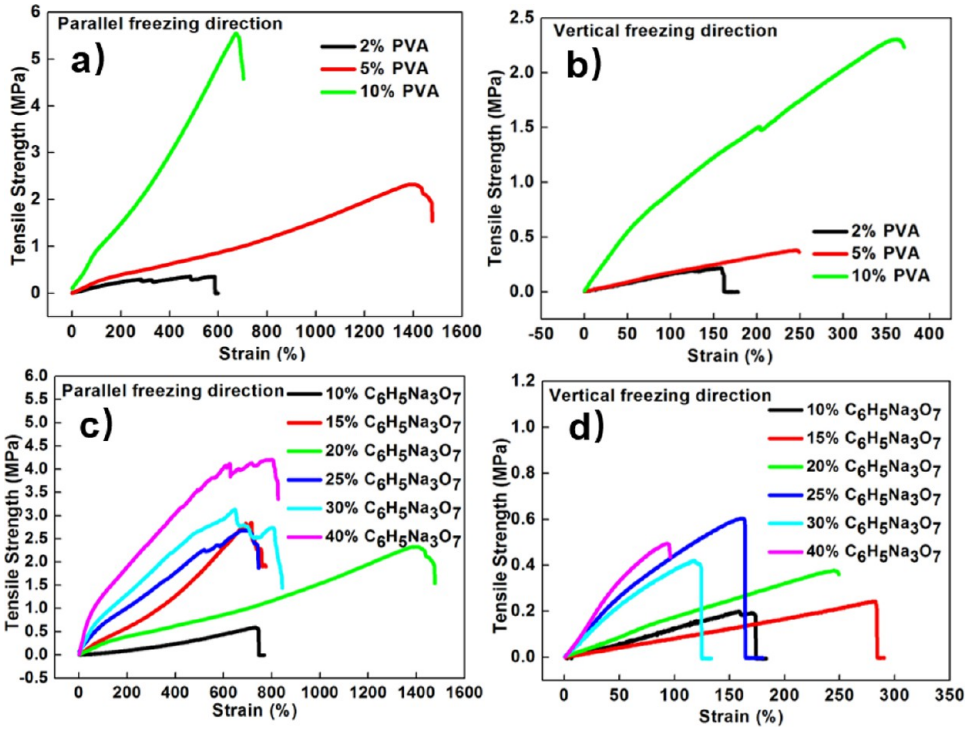

Figure 4. Stress−strain curves of the anisotropic hydrogel (DS-PVA) under different process conditions with parallel and vertical freezing directions. (a) Stress−strain curves of DS-PVA$_{\parallel}$ with different PVA concentrations; (b) stress−strain curves of DS-PVA$_{\perp}$ with different PVA concentrations; (c) stress−strain curves of DS-PVA$_{\parallel}$ with different salt concentrations; (d) stress−strain curves of DS-PVA$_{\perp}$ with different salt concentrations.

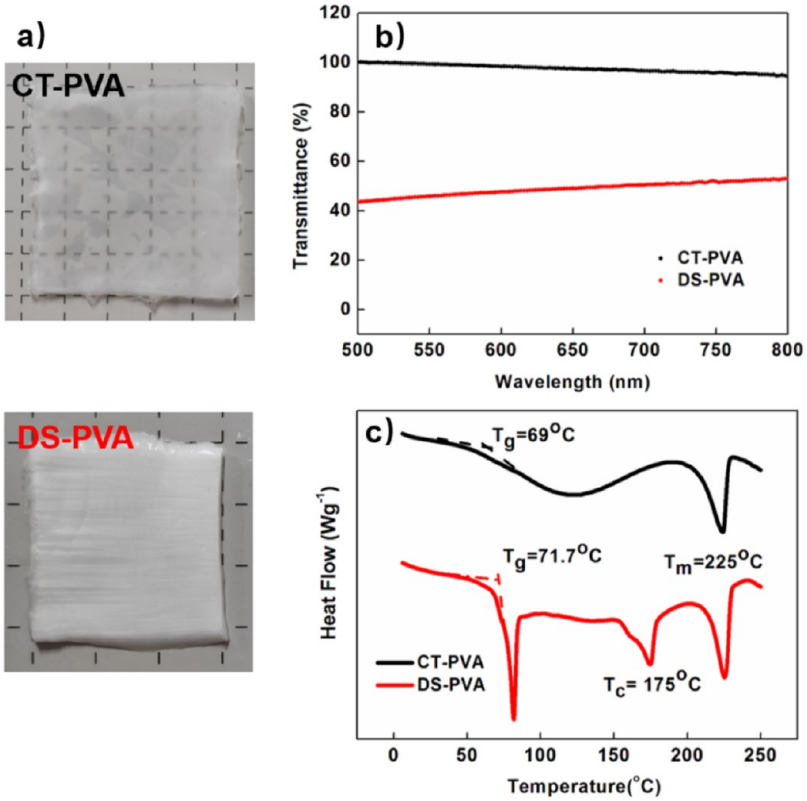

Figure 5. Comparative analysis of the hydrogel prepared by directional freezing versus salting-out and cyclic freezing−thawing methods. (a) Apparent contrast; (b) visible light transmittance analysis; (c) DSC analysis.

polymer aggregation clusters, while the salting-out effect induced the lower-scale aggregation structure control of such hydrogels. Moreover, the PVA and sodium citrate concentrations optimized the DS-PVA's ideal morphological structure

https://doi.org/10.1021/acsapm.3c01626
ACS Appl. Polym. Mater. 2023, 5, 9876−9887

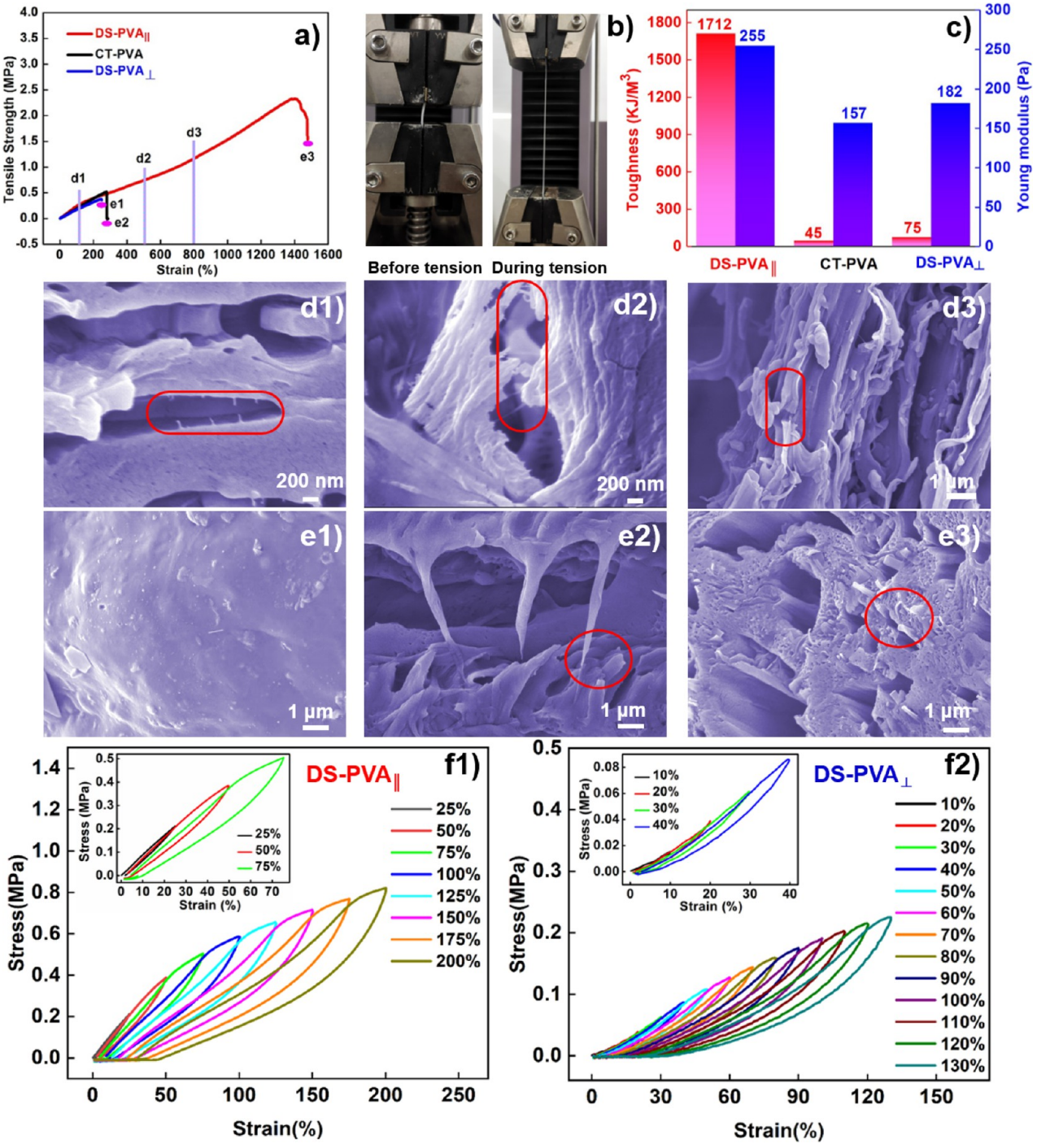

Figure 6. Mechanical performance of anisotropic (DS-PVA) and isotropic (CT-PVA) hydrogels prepared by directional freezing salting-out and cyclic freezing−thawing processes. (a) Stress−strain cures of hydrogels; (b) photograph of the DS-PVA$_{\parallel}$ before and after tension; (c) toughness and Young's modulus of hydrogels; (d1) SEM graph of DS-PVA$_{\parallel}$ with 100% strain; (d2) SEM graph of DS-PVA$_{\parallel}$ with 500% strain; (d3) SEM graph of DS-PVA$_{\parallel}$ with 800% strain; (e1) fracture morphology of CT-PVA; (e2) fracture morphology of DS-PVA$_{\perp}$; (e3) fracture morphology of DS-PVA$_{\perp}$; (f1) loading−unloading tensile tests of DS-PVA$_{\parallel}$; (f2) loading−unloading tensile tests of DS-PVA$_{\perp}$.

and mechanical performance. Figure 4 shows the stress−strain curves of DS-PVA under different process conditions with parallel and vertical directions. The tensile strength and Young's modulus of DS-PVA$_{\parallel}$ and DS-PVA$_{\perp}$ increased with PVA concentration in the same salt solution, while the strain showed the optimum value for a 5% PVA concentration (Figure 4a,b). Furthermore, the sodium citrate concentration also influenced the mechanical properties of DS-PVA. As shown in Figure 4c,d, the tensile strength and Young's modulus of DS-PVA$_{\parallel}$ and DS-PVA$_{\perp}$ increased with salt concentration, while the strain showed an ideal value with 20% sodium citrate. Therefore, the DS-PVA might obtain the best comprehensive mechanical properties in parallel and vertical freezing directions with 5% PVA and 20% sodium citrate.

The multiscale hierarchical anisotropic hydrogels were attributed to the strategy for adjusting and separating the PVA phase morphology. The PVA hydrogel (CT-PVA)

https://doi.org/10.1021/acsapm.3c01626
ACS Appl. Polym. Mater. 2023, 5, 9876−9887

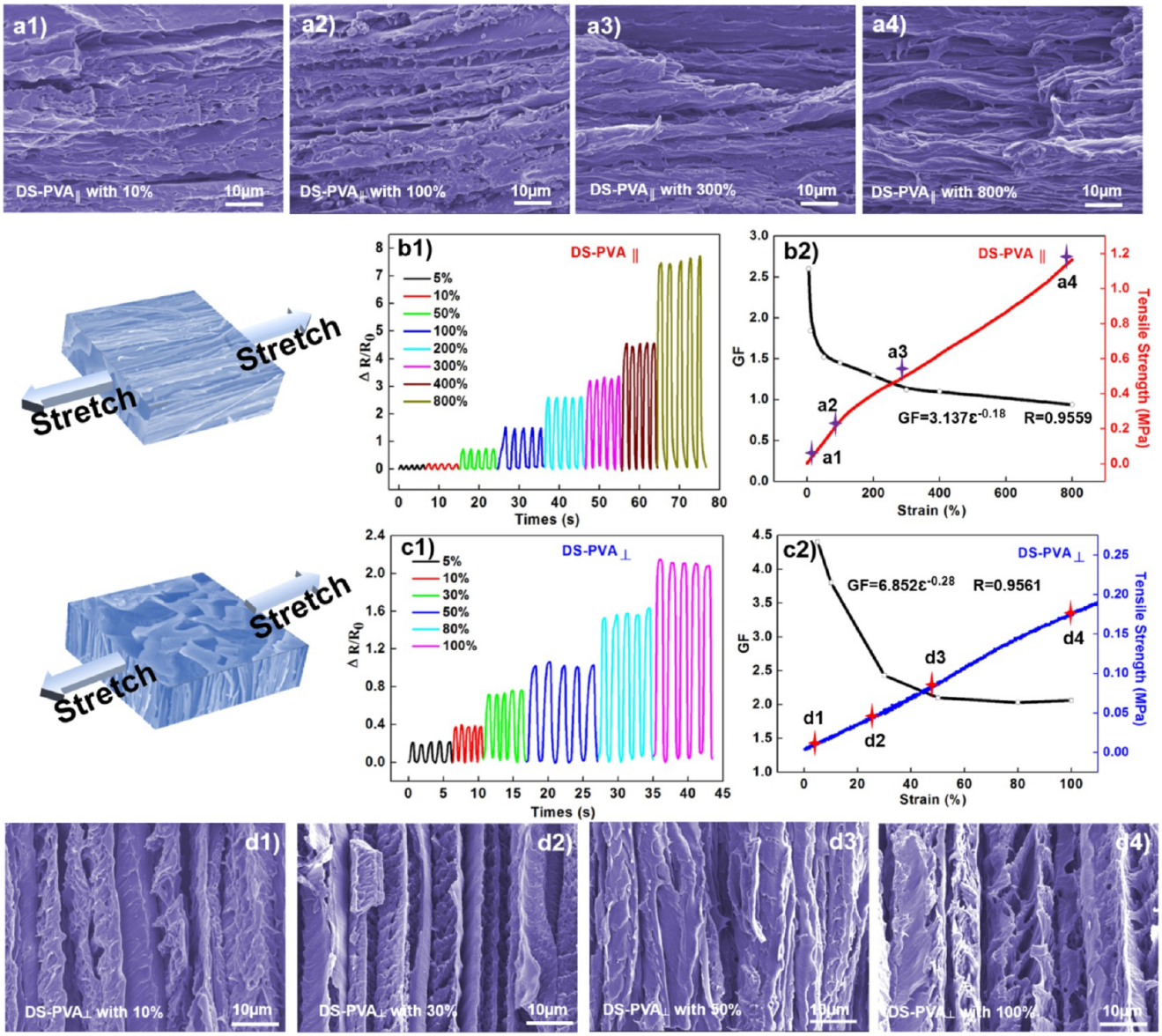

Figure 7. Strain electrical response behavior of the anisotropic hydrogel. (a) Morphologies of DS-PVA$_{\parallel}$ with different strains: (a1) 10%; (a2) 100%; (a3) 300%; (a4) 800%; (b1) cycling relative resistance variation with different strains for DS-PVA$_{\parallel}$; (b2) GF and stress variation with different strains for DS-PV$_{\parallel}$; (c1) cycling relative resistance variation with different strains for DS-PVA$_{\perp}$; (c2) GF and stress variation with different strains for DS-PVA$_{\perp}$; (d) morphologies of DS-PVA$_{\perp}$ with different strains: (d1) 10%; (d2) 30%; (d3) 50%; (d4) 100%.

fabricated by the traditional freezing−thawing method showed a homogeneous structure. Therefore, it was necessary to analyze the mechanical properties of DS-PVA and CT-PVA hydrogels and their structural morphology. Figure 5a shows the appearance of DS-PVA (5% PVA and 20% sodium citrate) and CT-PVA (5% PVA concentration). The CT-PVA showed obvious transparency, while DS-PVA was milky white. Moreover, the visible light transmittance spectrum of two kinds of hydrogels is shown in Figure 5b. The visible light transmittance of CT-PVA was almost 100%, while the transmittance of DS-PVA was only 43%. So, according to our experience, CT-PVA showed an amorphous structure, while DS-PVA prepared by directional freezing combined via the salting-out process exhibited a partially crystalline structure. From Figure 5c, the PVA hydrogel prepared by the cyclic freezing−thawing method (CT-PVA) showed two transition peaks: glass transition (marked as T_g) and melting (marked as T_m). The glass transition of CT-PVA showed lower and broader endothermal peaks compared with the T_g of DS-PVA. That indicated that the DS-PVA molecular chain arrangement was more orderly and regular, which required higher energy, inducing higher energy for structure change. And the distinct endotherm melting peaks could be observed at 225 °C for two types of hydrogels. Moreover, a new endothermic peak at 175 °C for DSC curves of DS-PVA demonstrated that the semicrystalline structure of DS-PVA melt recrystallized, while CT-PVA showed a typical amorphous structure. So, the directional freezing versus the salting-out process reconstructed the PVA crystal structure and increased crystallinity.[38]

Figure 6 shows the mechanical performance of anisotropic (DS-PVA) and isotropic (CT-PVA) hydrogels prepared by directional freezing salting-out and cyclic freezing−thawing processes. The tensile strength was Rm/DS-PVA$_{\parallel}$ = 2.35 MPa,

https://doi.org/10.1021/acsapm.3c01626
ACS Appl. Polym. Mater. 2023, 5, 9876−9887

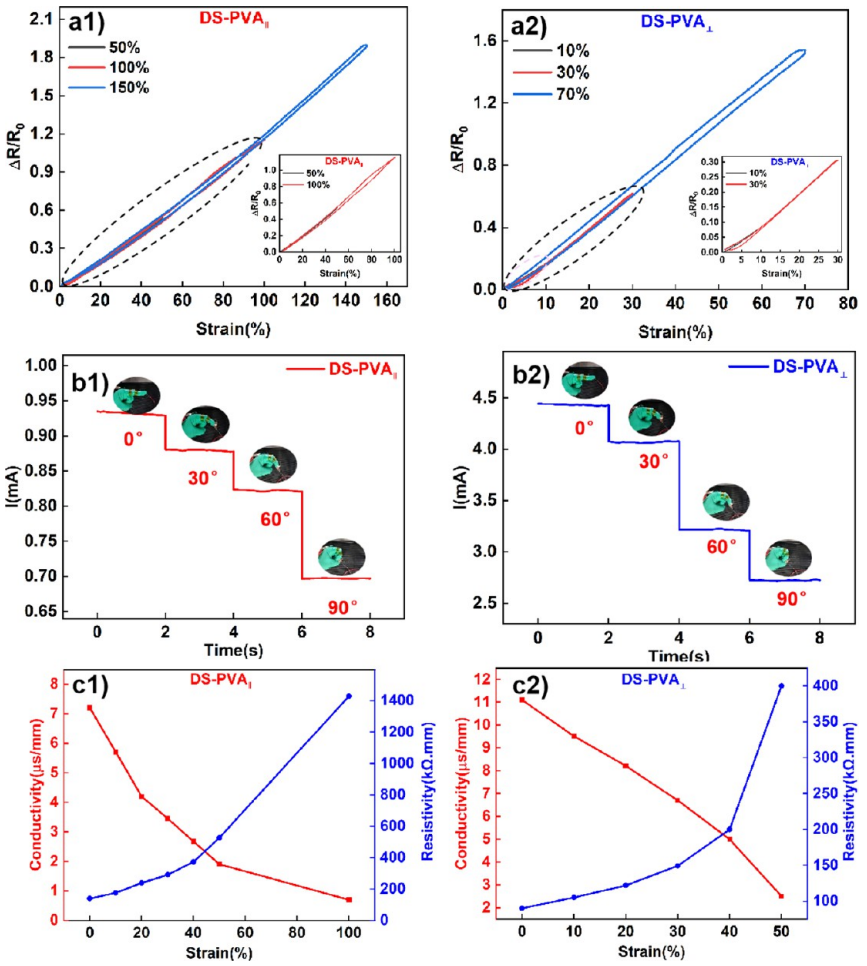

Figure 8. Asymmetric sensing mechanism of the multiscale hierarchical anisotropic hydrogel. (a1) Loading and unloading electrical response of DS-PVA$_\perp$; (a2) loading and unloading electrical response of DS-PVA$_\parallel$; (b1) bending from 0 to 90° current−time curves of DS-PVA$_\perp$; (b2) bending from 0 to 90° current−time curves of DS-PVA$_\parallel$; corresponding resistivity and electric conductivity; (c1) conductivity and resistivity curves for stretching DS-PVA$_\parallel$; (c2) conductivity and resistivity curves for stretching DS-PVA$_\perp$.

Rm/CT-PVA = 0.54 MPa, and Rm/DS-PVA$_\perp$ = 0.38 MPa (Figure 6a). So the Rm/DS-PVA$_\parallel$ was about 4.35 times for Rm/CT-PVA and 6.2 times for Rm/DS-PVA$_\perp$, which indicated that the DS-PVA after directional freezing versus salting-out method showed the higher strength feature in the parallel freezing direction. Moreover, the strain of DS-PVA$_\parallel$ was 1477%, far beyond that of CT-PVA and DS-PVA$_\perp$, demonstrating the super ductility in the parallel freezing direction. Figure 6b shows this point clearly. Young's modulus (E) could be calculated by the slope of linear elasticity 20−30% strain. The following formula could calculate toughness (U):

$$\text{Toughness } U = \int_0^{\varepsilon} \varepsilon \mathrm{d}\varepsilon \tag{1}$$

where U is the toughness (KJ/m^3) and ε is the strain (%).

Figure 6c shows the toughness (U) and Young's modulus (E) of hydrogels. The DS-PVA$_\parallel$ indicated excellent toughness with U = 1712 KJ/m^3, about 9.4 times U/DS-PVA$_\perp$. Young's modulus of DS-PVA$_\parallel$ was also increased to a certain extent compared with CT-PVA and DS-PVA$_\perp$. Therefore, the DS-PVA showed excellent strength, toughness, and stretchability in the freezing direction, which might be attributed to its special multiscale hierarchical anisotropic structure. From Figure 6d1−d3, the different scales of PVA aggregations (morphologies of DS-PVA$_\parallel$ with 100, 500, and 800% strain) oriented along with the tensile direction, resulting in the fibrosis structure. When the strain was 100%, the nanofibers broke up between the oriented aggregation to dissipate the energy (Figure 6d1). The submicron aggregation fractured with 500% strain, while large-scale microaggregation broke with 800% strain. In this way, DS-PVA$_\parallel$ could realize self-reinforcing and toughening by its structure. Furthermore, the fracture surface of CT-PVA showed a homogeneous and relatively brittle fracture morphology (Figure 6e1). However, the DS-PVA$_\parallel$ and DS-PVA$_\perp$ showed a multiscale hierarchical tough fracture, especially for DS-PVA$_\parallel$, and the fiber fracture structure at all levels appeared (Figure 6e2,e3).

As these multiscale hierarchy structures were believable to effectively dissipate the energy, we further analyzed the loading−unloading curves of DS-PVA in two freezing directions with different strains (Figure 6f1,f2). The DS-PVA$_\parallel$ showed efficient energy dissipation within 0−200% strain, while the DS-PVA$_\perp$ also got consistent results within 0−130% strain, which might be attributed to sacrificing a nanofiber structure. In addition, the curves showed good Mullins' effect in two freezing directions during the cycle loading−unloading with different strains.[39] Imaginably, these partially sacrificing nanofibers could efficiently dissipate energy without causing stress concentration, providing a sustained

https://doi.org/10.1021/acsapm.3c01626
ACS Appl. Polym. Mater. 2023, 5, 9876−9887

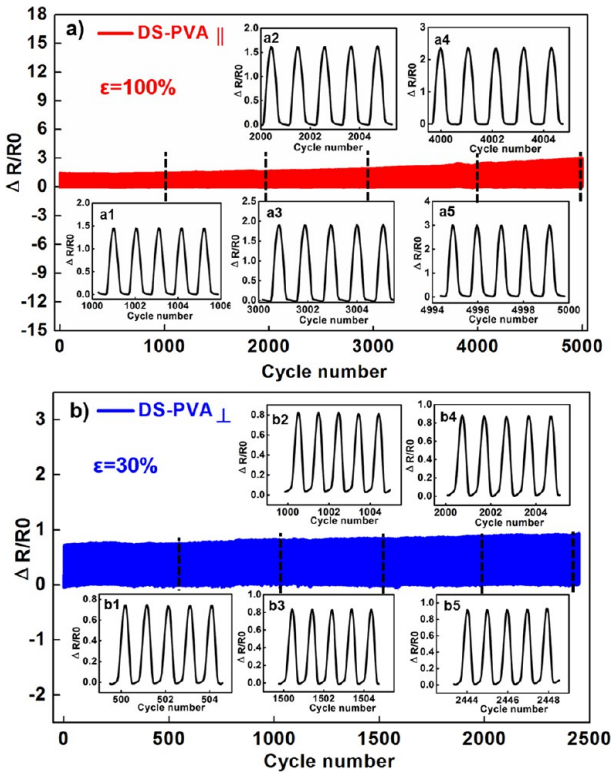

Figure 9. Cycling stability test for the anisotropic DS-PVA hydrogel. (a) Cycling stability test for DS-PVA$_{\parallel}$ with 100% strain; (b) cycling stability test for DS-PVA$_{\perp}$ with 30% strain.

toughening mechanism.[40] As shown in Figure S3, the DS-PVA$_{\parallel}$ showed good antifatigue characteristics after tens of thousands of loading and unloading with 10% strain. The loading and unloading curves shifted with the increase in the cycle number. The hydrogel materials were subjected to longer-term loading, and the internal molecular chain and cross-linking point failed to recover over time, resulting in a decrease in tensile stress. However, from the initial stage of cyclic loading and unloading to the end stage (Figure S3a1−a3), five loading and unloading curves in each stage almost overlap, showing good stability and fatigue resistance of the hydrogel material.

3.3. Relationship between Sensing Performance and Structure. Traditional ionically conductive hydrogels with 3D networks containing large free ions provided many stable channels for ion migration, realizing the mechanical−electronic response behavior.[41] When the ionic hydrogels suffered stress (stretch, press, and bend), the ionic hydrogels responded accordingly on the electrical signal diagram.[42] For isotropic hydrogels, the mechanical−electrical response exhibited isotropy.[43] Therefore, it was necessary to systematically analyze the sensing performance for such multiscale hierarchical anisotropic hydrogels.

As described above, DS-PVA had anisotropy on the mechanical properties and structural morphology. Based on this, we analyzed the mechanical−electronic properties of the device (Figure S5) in parallel and vertical freezing directions. Figure 7 shows the strain electrical response behavior of DS-PVA. From Figure 7b1,c1, the DS-PVA had different detection ranges, 0−800% for the parallel freezing direction and 0−100% for the vertical freezing direction. The relative change ($\Delta R/R_0$) increased with the strain increment. Moreover, the DS-PVA could realize five stable cycles with different strains in two freezing directions.

Sensitivity (gauge factor: GF) was an important factor value of the flexible sensor.[44] The GF showed a similar discipline, and the fitting curves presented power function characteristics with the strain, demonstrating negative characteristics (Figure 7b2,c2). The GF decreased dramatically at the lower strain, while GF decreased slowly with the strain increase. It was worth noting that the GF value of DS-PVA$_{\perp}$ was almost double that of DS-PVA$_{\parallel}$ at each corresponding strain, which was like different human bodies with different sensitivities under the same stimulus. The potential reason was that the DS-PVA$_{\perp}$ showed a multiscale porous hierarchical structure, while the DS-PVA$_{\parallel}$ showed a multiscale fibrosis hierarchical structure. So, the specific structure of DS-PVA would indeed affect its sensing mechanism. As shown in Figure 8b1,b2, the DS-PVA$_{\perp}$ direction had a higher initial current value. With the increase of the bending angles, the current of the hydrogel material showed a stepped attenuation and the DS-PVA$_{\perp}$ direction showed a higher responsivity. Similarly, the DS-PVA$_{\perp}$ direction showed a relatively higher conductivity and lower resistivity than DS-PVA$_{\parallel}$. Moreover, such hydrogels in both directions showed a similar variation with the strain increase, while the DS-PVA$_{\perp}$ indicated a more significant change in conductivity and resistivity (Figure 8c1,c2). As for the morphological structure difference between DS-PVA$_{\parallel}$ and DS-PVA$_{\perp}$, the hydrogels had significantly different ionic transfer channels in parallel and vertical freezing directions. Therefore, the sensing mechanism of such hydrogels showed obvious nonsymmetry in its sensing mechanism in two directions. Figure 8a1,a2 shows the curves of the resistance change rate during continuous loading−unloading of DS-PVA$_{\parallel}$ and DS-PVA$_{\perp}$. When DS-PVA$_{\parallel}$ and DS-PVA$_{\perp}$ suffered different loading and unloading strains, the $\Delta R/R_0$ stably increased with the strain increment and decreased with the strain reduction, forming the closed-loop curves of different strains. At the same time, the area between the loading curve and the unloading curve under different strains was small, which showed that hydrogel materials had low hysteresis in both directions and would not affect the stable use of hydrogel materials in sensing applications. All curves showed that the hydrogels' internal energy consumption and modulus remained stable during the load and unloading process, which indicated good device stability. Figure 7a1−a4 shows the morphologies of DS-PVA$_{\parallel}$ with different strains. When the DS-PVA$_{\parallel}$ suffered lower strain (0−100%), the multiscale fibrosis hierarchical structure was almost unchanged due to the linear elastic range (Figure 7a1,a2). When the strain was over 300%, the morphologies showed significant plastic deformation and increased fiber orientation degree (Figure 7a3,a4). Additionally, the DS-PVA$_{\perp}$ showed a linear elastic range from 0 to 50% with a consistent fiber aggregation parallel distribution structure (Figure 7d1−d3). As the strain was over 80%, the parallel spacing of fiber aggregates increased to a certain extent (Figure 7d4).

For response/recovery time, DS-PVA also showed some discrepancy characteristics in parallel and vertical freezing directions. The DS-PVA$_{\perp}$ had a faster response time of 127 ms and a recovery time of 63 ms with the 30% strain, while the DS-PVA$_{\parallel}$ showed a response of 232 ms and a recovery time of 84 ms, respectively (Figure S4a,b). DS-PVA had an anisotropy structure and different ion transfer channels inducing the response/recovery time diversity, similar to human skin and tissue with different tactile response thresholds. The antifatigue

https://doi.org/10.1021/acsapm.3c01626
ACS Appl. Polym. Mater. 2023, 5, 9876−9887

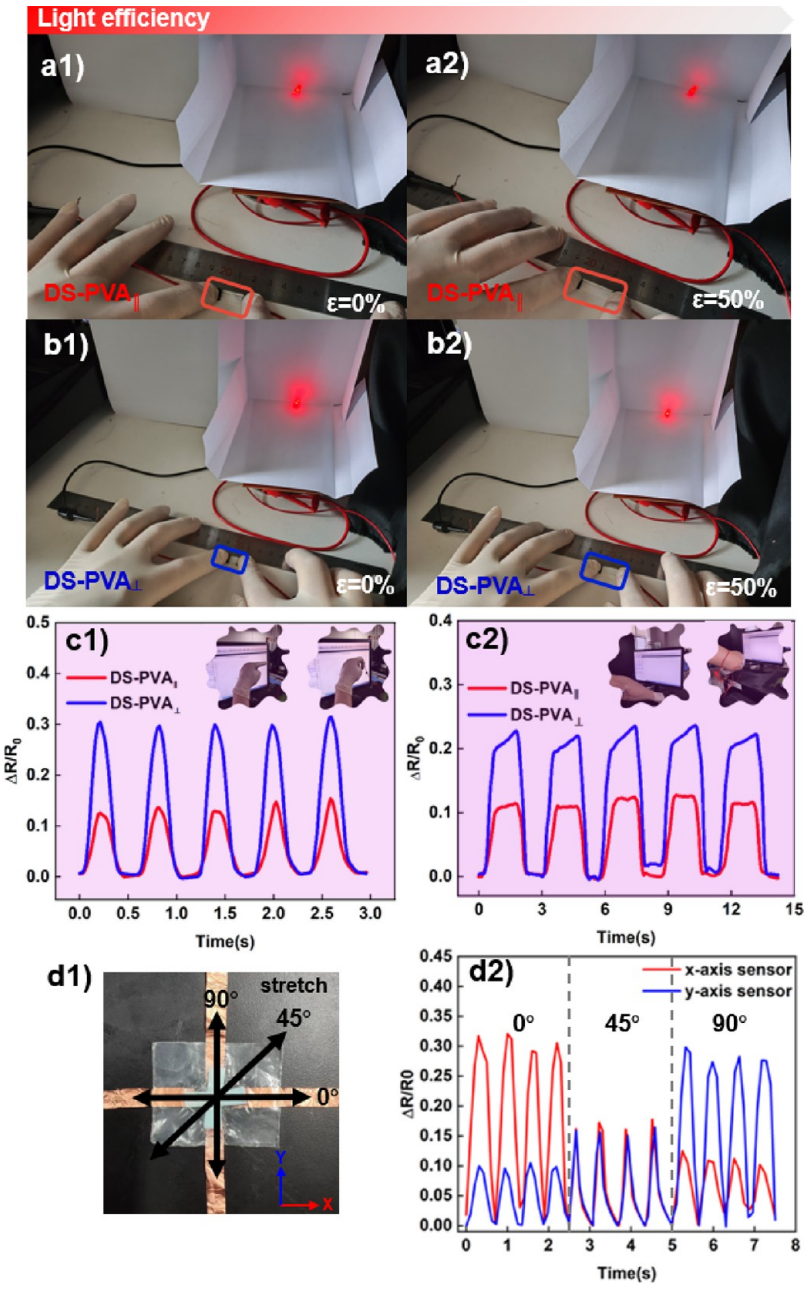

Figure 10. Sensing applications: (a1) LED brightness of DS-PVA$_{\parallel}$ with 0%; (a2) LED brightness of DS-PVA$_{\parallel}$ with 50%; (b1) LED brightness of DS-PVA$_{\perp}$ with 0%; (b2) LED brightness of DS-PVA$_{\perp}$ with 50%; (c1) finger bending with DS-PVA$_{\parallel}$ and DS-PVA$_{\perp}$; (c2) elbow bending with DS-PVA$_{\parallel}$ and DS-PVA$_{\perp}$; (d1) direction identification orthogonal strain sensor; (d2) sensing performance of the biaxial strain sensor under the 30% strains with stretch directions of 0, 45, and 90°.

and stability of the DS-PVA could be assessed by relative resistance change ($\Delta R/R_0$) for certain stretch and release cycles. The DS-PVA$_{\parallel}$ suffered over 5000 cycles under 100% strain, while the DS-PVA$_{\perp}$ withstood about 2500 cycles under 30% strain (Figure 9a,b). Therefore, the multiscale hierarchical anisotropy hydrogels different from the traditional hydrogels with unity stress-electrical response behavior showed an asymmetry and direction-selective sensing behavior similar to the human body to some extent.

Furthermore, some applications showed the asymmetry and directional selectivity of multiscale hierarchical anisotropic hydrogels in sensing mechanisms. Figure 10 shows some sensing applications for DS-PVA in two different freezing directions. The LED brightness of DS-PVA$_{\perp}$ was brighter than that of DS-PVA$_{\parallel}$ with 0% strain (Figure 10a1,b1) under the same working voltage, which indicated that the electron transport rate and the electron transport channel of DS-PVA in two freezing directions were different due to the anisotropy of the material structure. When we applied 50% strain, the LED brightness was weakened for DS-PVA$_{\parallel}$ and DS-PVA$_{\perp}$ (Figure 10b1,b2). The LED brightness attenuation in DS-PVA$_{\perp}$ was greater than that in DS-PVA$_{\parallel}$, indicating more sensitivity of DS-PVA$_{\perp}$ under the same amplitude strain. Moreover, some large-scale human motion identifications could be repeatably detected by DS-PVA$_{\parallel}$ and DS-PVA$_{\perp}$ (Figure 10c1,c2). Based on the sensing properties of this kind of hydrogel material, two identical DS-PVA$_{\parallel}$ specimens were combined with orthogonal stacking of the PVA orientation direction to form an

https://doi.org/10.1021/acsapm.3c01626
ACS Appl. Polym. Mater. 2023, 5, 9876−9887

orthogonal strain sensor, as shown in Figure 10d1. Such an orthogonal strain sensor fabricated by DS-PVA$_{\parallel}$ could provide effective strains in the orthogonal axes to realize direction recognition.[45] The electrical signals of the biaxial strain sensor stretched in different directions (0, 45, and 90°) were recorded under the cyclic 30% strain (Figure 10d2). When the stretching angle was 0° in the orthogonal system, the *X*-axis showed a higher signal, while the *Y*-axis showed a weaker signal. On the contrary, the electrical signal output of the *X*- and *Y*-axes was just the opposite when the stretching angle was 90°. Moreover, when the stretching angle was 45°, the two same-intensity electrical signal peaks were almost output on the *X*- and *Y*-axes. Therefore, the orthogonal strain sensor designed by this kind of multiscale hierarchical anisotropic hydrogel could accurately identify the strain in different directions by comparing the signal output of different amplitudes. The DS-PVA was similar to the human skin and tissue structure, so its sensing mechanism was asymmetry and directional selectivity, similar to tactile sensitivity and response speed of different parts of the human body. Therefore, such multiscale hierarchical anisotropic hydrogels might have potential application value in next generation wearable electronics.

4. CONCLUSIONS

In conclusion, we fabricated a multiscale hierarchical anisotropic hydrogel similar to human skin and tissue by directional freezing versus salting-out effect. The anisotropic morphology and multiple-graded structure resulted in the anisotropy of the mechanical properties and the asymmetry and directional selectivity of the sensing properties. The DS-PVA$_{\parallel}$ showed super strength, toughness, antifatigue, and wide sensing detection range characteristics, while the DS-PVA$_{\perp}$ showed high sensitivity and fast response/recovery time. Such multiscale hierarchical anisotropic hydrogels might apply to e-skin, flexible sensors, tissue engineering, and human−machine interfaces.

■ ASSOCIATED CONTENT

Supporting Information

The Supporting Information is available free of charge at https://pubs.acs.org/doi/10.1021/acsapm.3c01626.

DS-PVA 100% stretching for 5000 times cycles (video) (MP4)

Equipment that generates force stimulation: ball screw linear module; experimental apparatus for directional freezing; response and recovery times for the DS-PVA hydrogel; encapsulated hydrogel material and copper electrode for the test (PDF)

■ AUTHOR INFORMATION

Corresponding Authors

Xie Fu − *Key Laboratory of Multi-Scale Manufacturing Technology, Chongqing Institute of Green and Intelligent Technology, Chinese Academy of Sciences, Chongqing College, University of Chinese Academy of Sciences, Chongqing 400714, PR China; College of Mechanical Engineering, Chongqing University, Chongqing 400714, PR China;* orcid.org/0000-0002-2671-5464; Email: fuxie@cigit.ac.cn

Wenqiang Lu − *Key Laboratory of Multi-Scale Manufacturing Technology, Chongqing Institute of Green and Intelligent Technology, Chinese Academy of Sciences, Chongqing College, University of Chinese Academy of Sciences, Chongqing 400714, PR China*; Email: wqlu@cigit.ac.cn

Authors

Hui Tong − *Key Laboratory of Multi-Scale Manufacturing Technology, Chongqing Institute of Green and Intelligent Technology, Chinese Academy of Sciences, Chongqing College, University of Chinese Academy of Sciences, Chongqing 400714, PR China; School of Optoelectronic Engineering, Chongqing University of Posts and Telecommunications, Chongqing 400065, PR China*

Xia Zhang − *Key Laboratory of Multi-Scale Manufacturing Technology, Chongqing Institute of Green and Intelligent Technology, Chinese Academy of Sciences, Chongqing College, University of Chinese Academy of Sciences, Chongqing 400714, PR China*

Kun Zhang − *Key Laboratory of Multi-Scale Manufacturing Technology, Chongqing Institute of Green and Intelligent Technology, Chinese Academy of Sciences, Chongqing College, University of Chinese Academy of Sciences, Chongqing 400714, PR China*

Lyes Douadji − *Key Laboratory of Multi-Scale Manufacturing Technology, Chongqing Institute of Green and Intelligent Technology, Chinese Academy of Sciences, Chongqing College, University of Chinese Academy of Sciences, Chongqing 400714, PR China*

Shuai Kang − *Key Laboratory of Multi-Scale Manufacturing Technology, Chongqing Institute of Green and Intelligent Technology, Chinese Academy of Sciences, Chongqing College, University of Chinese Academy of Sciences, Chongqing 400714, PR China;* orcid.org/0000-0002-8174-8605

Jinling Luo − *Chongqing School, University of Chinese Academy of Sciences (UCAS Chongqing), Chongqing 400714, PR China*

Ziwei Pan − *Chongqing School, University of Chinese Academy of Sciences (UCAS Chongqing), Chongqing 400714, PR China*

Complete contact information is available at: https://pubs.acs.org/10.1021/acsapm.3c01626

Author Contributions

⊥X.F. and H.T. contributed as co-first authors.

Notes

The authors declare no competing financial interest.

■ ACKNOWLEDGMENTS

The authors thank the National Key R&D Program "Biology and Information Fusion (BT and IT Fusion)" Key Project (2022YFF1202002), the Chongqing Natural Science Foundation (no. cstc2021jcyj-msxmX1015), the Key Field Science and Technology Breakthrough Plan Project of Science and Technology Bureau of BINGTUAN (no. 2021AB026), and the Chongqing Talent, Innovation and Entrepreneurship Leading Talent Project (no. CQYC20210301363).

■ REFERENCES

(1) Hu, L.; Chee, P. L.; Sugiarto, S.; Yu, Y.; Shi, C.; Yan, R.; Yao, Z.; Shi, X.; Zhi, J.; Kai, D.; Yu, H.; Huang, W. Hydrogel-Based Flexible Electronics. *Adv. Mater.* **2023**, *35*, No. 2205326.

(2) Mondal, S.; Das, S.; Nandi, A. k. A Review on Recent Advances in Polymer and Peptide Hydrogels. *Soft Matter.* **2020**, *16*, 1404−1454.

(3) Peng, Q. Y.; Chen, J. S.; Wang, T.; Peng, X. W.; Liu, J. F.; Wang, X. G.; Wang, J. M.; Zeng, H. B. Recent advances in designing conductive hydrogels for flexible electronics. *InfoMater.* **2020**, *2*, 843−865.
(4) Yuk, H. W.; Wu, J. J.; Zhao, X. H. Hydrogel interfaces for merging humans and machines. *Nat. Rev. Mater.* **2022**, *7*, 935−952.
(5) Wu, Y. H.; Qu, J. K.; Zhang, X. H.; AO, K. L.; Zhou, Z. W.; Zheng, Z. Y.; Mu, Y. J.; Wu, X. Y.; Luo, Y.; Feng, S. P. Biomechanical Energy Harvesters Based on Ionic Conductive Organohydrogels via the Hofmeister Effffect and Electrostatic Interaction. *ACS Nano* **2021**, *15*, 13427−13435.
(6) Li, G.; Huang, K.; Deng, J.; Guo, M.; Cai, M.; Zhang, Y.; Guo, C. F. Highly Conducting and Stretchable Double-Network Hydrogel for Soft Bioelectronics. *Adv. Mater.* **2022**, *34*, No. 2200261.
(7) Yang, Y. Z.; Yuan, Y.; Zhang, G.; Wang, H.; Chen, Y. C.; Liu, Y. C.; Tarolli, C. G.; Crepeau, D.; Bukartyk, J.; Junna, M. R.; Videnovic, A.; Ellis, T. D.; Lipford, M. C.; Dorsey, R.; Katabi, D. Artificial intelligence-enabled detection and assessment of Parkinson's disease using nocturnal breathing signals. *Nat. Med.* **2002**, *28*, 2207−2215.
(8) Zhu, T.; Ni, Y.; Biesold, G. M.; Cheng, Y.; Ge, M.; Li, H.; Huang, J.; Lin, Z.; Lai, Y. Recent advances in conductive hydrogels: classifications, properties, and applications. *Chem. Soc. Rev.* **2023**, *52*, 473.
(9) Li, W.; Liu, J.; Wei, J.; Yang, Z.; Ren, C.; Li, B. Recent Progress of Conductive Hydrogel Fibers for Flexible Electronics: Fabrications, Applications, and Perspectives. *Adv. Funct. Mater.* **2023**, *33*, No. 2213485.
(10) Shen, B.; Peng, W. J.; Su, B. T.; Wu, L. Z.; Liu, Z. H.; Xu, H. H.; Zhao, J. X.; Feng, P. J.; Li, F. Y. Elastic−Electric Coefficient-Sensitive Hydrogel Sensors toward Sweat Detection. *Anal. Chem.* **2022**, *94*, 1910−1917.
(11) Wang, J.; Tang, F.; Yao, C.; Li, L. Low Hysteresis Hydrogel Induced by Spatial Confinement. *Adv. Funct. Mater.* **2023**, *33*, No. 2214935.
(12) Lei, K.; Li, Z.; Zhu, D. D.; Sun, C. Y.; Sun, Y. L.; Yang, C. C.; Zheng, Z.; Wang, X. L. Polysaccharide-Based Recoverable Double-Network Hydrogel with High Strength and Self-healing Property. *J. Mater. Chem. B* **2020**, *8*, 794−802.
(13) Jiang, P. P.; Qin, H. L.; Dai, J.; Yu, S. H.; Cong, H. P. Ultrastretchable and Self-Healing Conductors with Double Dynamic Network for Omni-Healable Capacitive Strain Sensors. *Nano Lett.* **2022**, *22*, 1433−1442.
(14) Ji, D.; Park, J. M.; Oh, M. S.; Nguyen, T. L.; Shin, H.; Kim, J. S.; Kim, D.; Park, H. S.; Kim, J. Superstrong, superstiff, and conductive alginate hydrogels. *Nat. Commun.* **2022**, *13*, 3019.
(15) Li, L.; Li, W.; Wang, X.; Zou, X.; Zheng, S.; Liu, Z.; Li, Q.; Xia, Q.; Yan, F. Ultra-Tough and Recyclable Ionogels Constructed by Coordinated Supramolecular Solvents. *Angew. Chem., Int. Ed.* **2022**, *61*, No. e202212512.
(16) Yang, T. T.; Xu, C.; Liu, C. L.; Ye, Y. Q.; Sun, Z. W.; Wang, B.; Luo, Z. Q. Conductive polymer hydrogels crosslinked by electrostatic interaction with PEDOT:PSS dopant for bioelectronics application. *Chem. Eng. J.* **2022**, *429*, No. 132430.
(17) Ye, Y.; Oguzlu, H.; Zhu, J.; Zhu, P.; Yang, P.; Zhu, Y.; Wan, Z.; Rojas, O. J.; Jiang, F. Ultrastretchable Ionogel with Extreme Environmental Resilience through Controlled Hydration Interactions. *Adv. Funct. Mater.* **2023**, *33*, No. 2209787.
(18) Zhang, X. Y.; Zeng, S.; Hu, Z. Y.; Liang, X.; Sun, Q.; Huang, J.; Zu, G. Q. Bioinspired Gradient Poly(ionic liquid) Ionogels for Ionic Skins with an Ultrawide Pressure Detection Range. *ACS Mater. Lett.* **2022**, *4*, 2459−2468.
(19) Wang, Y. Y.; Qin, H. L.; Li, Z.; Dai, J.; Cong, H. P.; Yu, S. H. Highly compressible and environmentally adaptive conductors with high-tortuosity interconnected cellular architecture. *Nat. Synth.* **2022**, *1*, 975−986.
(20) Yang, Y. F.; Wu, N.; Li, B.; Liu, W.; Pan, F.; Zeng, Z. H.; Liu, J. R. Biomimetic Porous MXene Sediment-Based Hydrogel for High-Performance and Multifunctional Electromagnetic Interference Shielding. *ACS Nano* **2022**, *16* (9), 15042−15052.
(21) Li, W.; Tao, L. Q.; Kang, M. C.; Li, C. H.; Luo, C. Y.; He, G.; Sang, T. Y.; Wang, P. Tunable mechanical, self-healing hydrogels driven by sodium alginate and modified carbon nanotubes for health monitoring. *Carbohydr. Ploym.* **2022**, *295*, No. 119854.
(22) Wang, Z. W.; Wei, H.; Huang, Y. J.; Wei, Y.; Chen, J. Naturally sourced hydrogels: emerging fundamental materials for next-generation healthcare sensing. *Chem. Soc. Rev.* **2023**, *52*, 2992−3034.
(23) Morales, D.; Bharti, B.; Dickey, M. D.; Velev, O. D. Bending of Responsive Hydrogel Sheets Guided by Field Assembled Microparticle Endoskeleton Structures. *Small.* **2016**, *12*, 2283−2290.
(24) Liu, M. J.; Ishida, Y.; Ebina, Y.; Sasaki, T.; Hikima, T.; Takata, M.; Aida, T. An anisotropic hydrogel with electrostatic repulsion between cofacially aligned nanosheets. *Nature.* **2015**, *517*, 68−72.
(25) Mredha, M. T. I.; Guo, Y. Z.; Nonoyama, T.; Nakajima, T.; Kurokawa, T.; Gong, J. P. Facile Method to Fabricate Anisotropic Hydrogels with Perfectly Aligned Hierarchical Fibrous Structures. *Adv. Mater.* **2018**, *30*, No. 1704937.
(26) Wang, C. L.; Chai, Y.; Wen, X. D.; Ai, Y. J.; Zhao, H.; Hu, W. T.; Yang, X. P.; Ding, X. Y.; Shi, X. L.; Liu, Q. F.; Liang, Q. L. Stretchable and Anisotropic Conductive Composite Hydrogel as Therapeutic Cardiac Patches. *ACS. Materials. Lett.* **2021**, *3*, 1238−1248.
(27) Yang, G.; Tang, X. C.; Zhao, G. D.; Li, Y. F.; Ma, C. Q.; Zhuang, X. P.; Yan, J. Highly sensitive, direction-aware, and transparent strain sensor based on oriented electrospun nanofibers for wearable electronic applications. *Chem. Eng. J.* **2022**, *435*, No. 135004.
(28) Dong, X.; Guo, X.; Liu, Q.; Zhao, Y.; Qi, H.; Zhai, W. Strong and Tough Conductive Organo-Hydrogels via Freeze-Casting Assisted Solution Substitution. *Adv. Funct. Mater.* **2022**, *32*, No. 2203610.
(29) Liang, X.; Chen, G.; Lin, S.; Zhang, J.; Wang, L.; Zhang, P.; Wang, Z.; Wang, Z.; Lan, Y.; Ge, Q.; Liu, J. Anisotropically Fatigue-Resistant Hydrogels. *Adv. Mater.* **2021**, *33*, No. 2102011.
(30) Zhu, W. Z.; Wang, J.; Sun, W.; Zhou, S.; He, M. Preparation of gradient hydrogel for pressure sensing by combining freezing and directional diffusion processes. *Chem. Eng. J.* **2023**, *451*, No. 138335.
(31) Guo, X.; Dong, X.; Zou, G.; Gao, H.; Zhai, W. Strong and tough fibrous hydrogels reinforced by multiscale hierarchical structures with multimechanisms. *Sci. Adv.* **2023**, *9*, No. eadf7075.
(32) Hua, M.; Wu, S.; Ma, Y.; Zhao, Y.; Chen, Z.; Frenkel, I.; Strzalka, J.; Zhou, H.; Zhu, X.; He, X. Strong tough hydrogels via the synergy of freeze-casting and salting out. *Nature* **2021**, *590*, 594−606.
(33) Cai, J. H.; Chen, Y. F.; Li, J.; Tan, Y. J.; Liu, J. H.; Tang, X. H.; Chen, X. D.; Wang, M. Asymmetric Deformation in Poly(ethylene-co-1-octene)/Multi-Walled Carbon Nanotube Composites with Glass Micro-Beads for Highly Piezoresistive Sensitivity. *Chem. Eng. J.* **2019**, *370*, 176−184.
(34) Cai, J. H.; Li, J.; Chen, X. D.; Wang, M. Multifunctional Polydimethylsiloxane Foam with Multi-Walled Carbon Nanotube and Thermo-Expandable Microsphere for Temperature sensing, Microwave Shielding and Piezoresistive Sensor. *Chem. Eng. J.* **2020**, *393*, No. 124805.
(35) Cui, W.; Zheng, Y.; Zhu, R.; Mu, Q.; Wang, X.; Wang, Z.; Liu, S.; Li, M.; Ran, R. Strong Tough Conductive Hydrogels via the Synergy of Ion-Induced Cross-Linking and Salting-Out. *Adv. Funct. Mater.* **2022**, *32*, No. 2204823.
(36) Wu, S.; Wang, T. W.; Du, Y.; Yao, B.; Duan, S.; Yan, Y.; Hua, M.; Alsaid, Y.; Zhu, X.; He, X. Tough, anti-freezing and conductive ionic hydrogels. *NPG Asia Mater.* **2022**, *65*, 1−8.
(37) Li, J.; Li, J.; Tang, Y.; Liu, Z.; Zhang, Z.; Wu, H.; Shen, B.; Su, M.; Liu, M.; Li, F. Touchable Gustation via a Hoffmeister Gel Iontronic Sensor. *ACS Nano* **2023**, *5*, 5129−5139.
(38) Xu, L.; Qiao, Y.; Qiu, D. Coordinatively Stiffen and Toughen Hydrogels with Adaptable Crystal-Domain Cross-Linking. *Adv. Mater.* **2023**, *35*, No. 2209913.
(39) Yang, C. H.; Yin, T. H.; Suo, Z. G. Polyacrylamide hydrogels. I. Network imperfection. *J. Mech. Phys. Solids.* **2019**, *131*, 43−55.

https://doi.org/10.1021/acsapm.3c01626
ACS Appl. Polym. Mater. 2023, 5, 9876−9887

(40) Bai, R.; Yang, J.; Morelle, X. P.; Suo, Z. Flaw-Insensitive Hydrogels under Static and Cyclic Loads. *Macromol. Rapid Commun.* **2019**, *40*, No. 1800883.
(41) Wang, L. R.; Xu, T. L.; Zhang, X. J. Multifunctional conductive hydrogel-based flexible wearable sensors. *Trac-Trend. Anal. Chem.* **2021**, *134*, No. 116130.
(42) Li, G.; Li, C.; Li, G.; Yu, D.; Song, Z.; Wang, H.; Liu, X.; Liu, H.; Liu, W. Development of Conductive Hydrogels for Fabricating Flexible Strain Sensors. *Small* **2022**, *18*, No. 2101518.
(43) Tie, J. F.; Mao, Z. P.; Zhang, L. P.; Zhong, Y.; Sui, X. F.; Xu, H. Highly sensitive, durable, environmentally tolerant and multimodal composite ionogel-based sensor with an ultrawide response range. *Sci. China. Mater.* **2023**, *66*, 1899−1910.
(44) Guo, B.; He, S.; Yao, M.; Tan, Z.; Li, X.; Liu, M.; Yu, C.; Liang, L.; Zhao, Z.; Guo, Z.; Shi, M.; Wei, Y.; Zhang, H.; Yao, F.; Li, J. MXene-containing anisotropic hydrogels strain sensors with enhanced sensing performance for human motion monitoring and wireless transmission. *Chem. Eng. J.* **2023**, *463*, No. 142099.
(45) Yang, G.; Tang, X. X.; Zhao, G. D.; Li, Y. F.; Ma, C. Q.; Zhuang, X. P.; Yan, J. Highly sensitive, direction-aware, and transparent strain sensor based on oriented electrospun nanofibers for wearable electronic applications. *Chem. Eng. J.* **2022**, *435*, No. 135004.

https://doi.org/10.1021/acsapm.3c01626
ACS Appl. Polym. Mater. 2023, 5, 9876−9887